Asociación Argentina
de Mecánica Computacional

Mecánica Computacional Vol XXXIV, págs. 3619-3635 (artículo completo)
Sebastián Giusti, Martín Pucheta y Mario Storti (Eds.)
Córdoba, 8-11 Noviembre 2016

CALCULATION OF THE CROSS SECTIONAL PROPERTIES OF LARGE WIND TURBINE BLADES

Martín Saravia[a,b]

[a]*Grupo de Investigación en Multifísica Aplicada, CONICET – Universidad Tecnológica Nacional, Facultad Regional Bahía Blanca, 11 de Abril 461, 8000 Bahía Blanca, Argentina.*

[b]*Centro de Investigación en Mecánica Teórica y Aplicada, CONICET – Universidad Tecnológica Nacional, Facultad Regional Bahía Blanca, 11 de Abril 461, 8000 Bahía Blanca, Argentina.*

Keywords: Wind turbines, Composite materials, Finite elements, thin-walled beams, cross section

Abstract. This paper presents a computational approach for the calculation of the mechanical properties of large wind turbine blades. The relation between the geometric discretization of anisotropic cross sections via line elements and the calculation of its mechanical properties is analyzed. The composite material theoretical background is based on a vector variant of the classical lamination theory embedded into a geometrically exact large deformation-small strain thin-walled beam formulation; transverse shear and out of plane warping are considered. The impact of the geometric reconstruction on the accuracy of the mechanical properties is studied using both rectangular and trapezoidal elements. It is shown that line based algorithms can give very accurate results provided the cross section geometry is well represented.

1 INTRODUCTION

Computational modeling of composite wind turbine blades is a hot research subject (UpWind, 2011, Spera, 2009, Jonkman et al., 2009, Hansen, 2008, Hansen et al., 2006, Hau, 2006); both 3D, 2D and 1D modeling techniques have been investigated in the last years. Most modern approaches make use of finite elements, so the response of the blade is typically computed after some kind of discretization. In the most general case, the full blade can be discretized into solid finite elements; however, this three dimensional modeling technique is rarely used since the time required to generate such a complex geometry is prohibitive. Besides, the aeroelastic nature of the wind turbine blade dynamics makes a full fluid-structure 3D simulation using solid elements almost impossible to execute. This opens the possibility for a wide variety of the so-called "reduced theories", which make use of various hypotheses to model the structural behavior of the blade; these hypothesis permits the simplification of its geometrical representation and mechanical behavior.

Three approaches are used to simulate the mechanics of composite wind turbine blades: *i)* 3D shell approaches, where the outer surface of the blade is discretized into tridimensional surface elements of composite material that deform arbitrarily in space (Laird, 2001). The geometrical errors arising from the definition of the cross section as a set of shell elements cannot be avoided; although, the accuracy of the method is generally good (Saravia et al., 2015a), *ii)* coupled surface-line algorithms (SLAs), where the blade is conceived as a set of cross sections modeled as 2D surface elements; the group of cross sections move solidary to a reference 1D curve that deforms in space following the laws of a certain beam theory (Cesnik and Hodges, 1997, Chen et al., 2010, Hodges and Yu, 2007). This is probably the most accurate approach to describe the mechanic behavior of the blade since the cross sectional modeling with 2D elements permits a fine description of the blade geometric constructive details; also, the cross sectional algorithm can be coupled with almost any beam theory and *iii)* coupled line-line algorithms (LLAs), where the blade is conceived as a set of cross sections modeled as line elements; the group of cross sections move solidary to a reference 1D curve that deforms in space following the laws of a certain beam theory (Cesnik and Hodges, 1997, Chen et al., 2010, Hodges and Yu, 2007). The accuracy of the LLAs is dependent on the geometrical reconstruction algorithm and the composite material mechanical description. The accuracy of modern LLAs is very good; for certain cross sections LLA can give more accurate results than 3D shell approaches (Saravia et al., 2015a).

SLAs are more accurate than LLAs; however, LLAs still have a number of advantages over SLAs: i) low time consumption and fast execution, ii) capacity of handling very small thickness layers of paint and coating and iii) flexibility to be coupled easily with general heuristic optimization software without implying a generation of a new mesh.

LLAs are widely used in rotor design to determine the cross sectional stiffness of blade. Chen et. al (Chen et al., 2010) presented a detailed assessment of the most used computational tools for calculating wind turbine blade cross sectional stiffness. This study includes numerical comparisons between: analytic results, the SLA VABS (Variational Asymptotic Beam Section Analysis, the most renowned algorithm for the determination of cross sectional properties, developed by Prof. Hodges and coworkers (Hodges and Yu, 2007, Cesnik and Hodges, 1997, Yu et al., 2002)) and the LLAs: FAROB (Philippidis et al., 1996) (developed at the Dutch Knowledge Center of Wind Energy Materials and Construction), PreComp (Bir, 2005) (developed at National Renewable Energy Laboratory in USA) and CROSTAB (Lindenburg, 2008) (developed at the Energy Research Center of the Netherlands). The study concludes that the LLAs are inconsistent and therefore its applicability to modeling realistic blades is questionable; the present paper aims to show that this conclusion is misleading.

Resor et. al (Resor et al., 2010) compared results obtained with PreComp and BPE (a 3D shell approach developed by Global Energy Concepts and Sandia National Laboratories (Malcolm and Laird, 2007)), to those obtained in experimental testing of the BSDS blade; according to this paper the overall difference between PreComp and BPE is in the range of 15-25% and the difference between the experimental results and BPE are in the range of 5-20%. In a later study, Resor and Paquette also included VABS in the assessment of the cross sectional stiffness calculation (Resor and Paquette, 2011). The paper reproduced the same results of (Chen et al., 2010) for a particular wind turbine cross section, only the diagonal terms of the stiffness matrix were presented. For the CX-100 blade, discrepancies were found between VABS and BPE, especially in sections near the blade's root. These discrepancies were attributed to local straining.

This work presents a computational approach based on a LL formulation to obtain the cross sectional properties of wind turbine blades. A similar version of a previously presented LLA (Saravia et al., 2015a) is used to analyze the impact of the discretization aspects on the accuracy of the results. The geometric reconstruction of the cross sections is done with two types of segments, classical thin-walled beam theory rectangular segments and a variable layer length trapezoidal segment. It will be shown that the choice of the reconstruction element greatly affects the prediction of the cross sectional parameters.

2 THEORETICAL ASPECTS

2.1 Beam Formulation

A particular cross sectional stiffness measure is consistent only with the kinematic formulation from which it was derived. The full derivation of the composite beam formulation used in this paper can be found in (Saravia et al., 2015a, Saravia, 2014); only the relevant details are reproduced hereafter. It is assumed that the mechanic behavior of the blade can be approximated by beam theory.

The position vector of a point in the blade in the undeformed and deformed configuration can respectively be expressed as

$$\begin{aligned} \boldsymbol{X}(x,\xi_2,\xi_3) &= \boldsymbol{X}_0(x) + \sum_{i=2}^{3} \xi_i \, \boldsymbol{E}_i, \\ \boldsymbol{x}(x,\xi_2,\xi_3,t) &= \boldsymbol{x}_0(x,t) + \sum_{i=2}^{3} \xi_i \, \boldsymbol{e}_i + \omega \, \boldsymbol{e}_1. \end{aligned} \tag{1}$$

where $\boldsymbol{X}_0$ and $\boldsymbol{x}_0$ stand for the position of the pole in the undeformed and deformed configurations respectively and the second term stands for the position of a point within the cross section relative to the pole; the coordinates ξ_2 and ξ_3 are the components of the position vector of a point in the cross section in $\boldsymbol{E}_i$. The variable ω accounts for the displacements in the cross section due to torsional warping.

Three frames of reference attached to the cross section are introduced: a) a reference material frame $\{\boldsymbol{E}_1, \boldsymbol{E}_2, \boldsymbol{E}_3\}$, b) a sectional frame $\{\boldsymbol{E}_1, \hat{\boldsymbol{n}}, \hat{\boldsymbol{s}}\}$ and c) a layer individual frame $\{\hat{\mathbf{1}}, \hat{\mathbf{2}}, \hat{\mathbf{3}}\}$, see (Saravia, 2014).

The Small Green Strain Tensor (SGS) tensor can be written in vector form as (Saravia et al., 2015b)

$$\boldsymbol{e} = \begin{bmatrix} \boldsymbol{x}_0' \cdot \boldsymbol{e}_1 - 1 + \xi_\alpha \boldsymbol{e}_\alpha' \cdot \boldsymbol{e}_1 \\ \boldsymbol{x}_0' \cdot \boldsymbol{e}_2 + \xi_3 \boldsymbol{e}_3' \cdot \boldsymbol{e}_2 \\ \boldsymbol{x}_0' \cdot \boldsymbol{e}_3 + \xi_2 \boldsymbol{e}_2' \cdot \boldsymbol{e}_3 \end{bmatrix}. \tag{2}$$

In vector form

$$\boldsymbol{e} = \boldsymbol{D}\boldsymbol{\varepsilon}, \tag{3}$$

being $\boldsymbol{D}$ a cross sectional matrix such that

$$\boldsymbol{D} = \begin{bmatrix} \boldsymbol{E}_1 & \boldsymbol{r} \\ \boldsymbol{E}_2 & \boldsymbol{r} \times \boldsymbol{E}_2 \\ \boldsymbol{E}_3 & \boldsymbol{r} \times \boldsymbol{E}_3 \end{bmatrix}, \tag{4}$$

and $\boldsymbol{\varepsilon}$ the generalized strain vector.

$$\boldsymbol{\varepsilon} = \begin{bmatrix} \boldsymbol{x}_0' \cdot \boldsymbol{e}_1 - 1 \\ \boldsymbol{x}_0' \cdot \boldsymbol{e}_2 \\ \boldsymbol{x}_0' \cdot \boldsymbol{e}_3 \\ \boldsymbol{e}_2' \cdot \boldsymbol{e}_3 \\ \boldsymbol{e}_2' \cdot \boldsymbol{e}_1 \\ \boldsymbol{e}_3' \cdot \boldsymbol{e}_1 \end{bmatrix}. \tag{5}$$

Lastly, the curvature and axial-shear strain vectors are defined for future use as

$$\begin{aligned} \boldsymbol{\gamma} &= [\epsilon \quad \gamma_2 \quad \gamma_3]^T = [\boldsymbol{x}_0' \cdot \boldsymbol{e}_1 - 1 \quad \boldsymbol{x}_0' \cdot \boldsymbol{e}_2 \quad \boldsymbol{x}_0' \cdot \boldsymbol{e}_3]^T, \\ \boldsymbol{\kappa} &= [\kappa_1 \quad \kappa_2 \quad \kappa_3]^T = [\boldsymbol{e}_2' \cdot \boldsymbol{e}_3 \quad \boldsymbol{e}_2' \cdot \boldsymbol{e}_1 \quad \boldsymbol{e}_3' \cdot \boldsymbol{e}_1]^T. \end{aligned} \tag{6}$$

Then the generalized strain vector can be written in the form

$$\boldsymbol{\varepsilon} = [\boldsymbol{\gamma}^T \quad \boldsymbol{\kappa}^T]^T. \tag{7}$$

2.2 The sectional strain measures

In order to write the constitutive equations it is necessary to express the SGS in the cross sectional frame $\{\boldsymbol{E}_1, \hat{\boldsymbol{n}}, \hat{\boldsymbol{s}}\}$. Recall that the origin of the cross sectional system moves along the cross section contour (placed half a thickness inward from the outer contour) in anticlockwise direction; then the tangent unit vector can be found as the derivative of the mid-contour position vector $\bar{\boldsymbol{r}} = \bar{\xi}_2 \boldsymbol{E}_2 + \bar{\xi}_3 \boldsymbol{E}_3$. This is

$$\hat{\boldsymbol{s}} = \frac{d\bar{\boldsymbol{r}}}{ds} = \bar{\xi}_2' \boldsymbol{E}_2 + \bar{\xi}_3' \boldsymbol{E}_3, \tag{8}$$

where $\bar{\xi}_i'$ represents derivatives of mid-contour cross sectional coordinates with respect to s. The normal unit vector can be obtained invoking the orthogonality condition of the coordinate system, then

$$\hat{\boldsymbol{n}} = \hat{\boldsymbol{s}} \times \boldsymbol{E}_1 = \bar{\xi}_3' \boldsymbol{E}_2 - \bar{\xi}_2' \boldsymbol{E}_3. \tag{9}$$

The position vector of a point in the cross section expressed in the sectional coordinate system is

$$\boldsymbol{r}_s = (\bar{r}_n + n)\hat{\boldsymbol{n}} + \bar{r}_s\hat{\boldsymbol{s}},$$
$$\bar{\boldsymbol{r}}_s = \bar{r}_n\hat{\boldsymbol{n}} + \bar{r}_s\hat{\boldsymbol{s}}, \tag{10}$$

where the mid-contour components are obtained as

$$\bar{r}_n = \bar{\boldsymbol{r}}_s \cdot \hat{\boldsymbol{n}} = \xi_2\bar{\xi}_3' - \xi_3\bar{\xi}_2',$$
$$\bar{r}_s = \bar{\boldsymbol{r}}_s \cdot \hat{\boldsymbol{s}} = \xi_2\bar{\xi}_2' + \xi_3\bar{\xi}_3'. \tag{11}$$

Another needed relation is the position of a point in the cross section as a function of the mid-contour coordinates, this is

$$\boldsymbol{r} = \bar{\boldsymbol{r}} + n\hat{\boldsymbol{n}} = \left(\bar{\xi}_2 + n\bar{\xi}_3'\right)\boldsymbol{E}_2 + \left(\bar{\xi}_3 - n\bar{\xi}_2'\right)\boldsymbol{E}_3. \tag{12}$$

Now, a sectional frame transformation tensor $\boldsymbol{Q}_s$ is introduced (see (Saravia et al., 2015b)), it operates over the SGS tensor to give the strains in the sectional system as

$$\boldsymbol{e} = \boldsymbol{Q}_s^T\boldsymbol{E}\boldsymbol{Q}_s; \tag{13}$$

The SGS expressed in the sectional frame is

$$\boldsymbol{e}_s = \begin{bmatrix}\epsilon_x \\ \gamma_{xs} \\ \gamma_{xn}\end{bmatrix} = \begin{bmatrix}\epsilon + \left(\kappa_3\bar{\xi}_2 + \kappa_2\bar{\xi}_3\right) + n\left(\kappa_3\bar{\xi}_3' - \kappa_2\bar{\xi}_2'\right) \\ \left(\bar{\xi}_2'\gamma_2 + \bar{\xi}_3'\gamma_3\right) + \kappa_1 r_n \\ \left(\bar{\xi}_3'\gamma_2 - \bar{\xi}_2'\gamma_3\right) - \kappa_1\bar{r}_s\end{bmatrix}, \tag{14}$$

The last equation can be written as a function of the generalized strains as

$$\boldsymbol{e}_s = \boldsymbol{D}_s\boldsymbol{\varepsilon} = \begin{bmatrix}\boldsymbol{1} & \boldsymbol{r} \\ \hat{\boldsymbol{s}} & r_n\boldsymbol{1} \\ \hat{\boldsymbol{n}} & -\bar{r}_s\boldsymbol{1}\end{bmatrix}\begin{bmatrix}\boldsymbol{\gamma} \\ \boldsymbol{\kappa}\end{bmatrix} \tag{15}$$

where $r_n = \bar{r}_n + n$.

3 BLADE MODELING

A wind turbine blade is built by two types of materials: the ones which contribute with mass, the ones which contribute with mass and stiffness. The former includes coating, painting and filling materials; filling materials have very low stiffness and are used mainly to increase the local buckling stiffness at some specific locations. The latter includes all composites, fabrics, etc. From the computational point of view, the materials not contributing to stiffness do not pass through the stiffness algorithms. This is convenient not only because the stiffness matrix computation is faster but also because problems arising from poor local vector conditioning due to the extremely small thicknesses of paint and coatings are avoided.

The use of filling materials such as foam or balsa is used in a sandwich-like configuration. This scheme improves the local stiffness at the expense of a minor decrease in global stiffness and a major increase in the local thickness of the laminate. The latter renders the cross section thick-walled, what may have two consequences: i) the normal stresses in the thick-walled segment are not necessarily small and ii) the length of the inner layers of the laminate is less than the length of the outer layers. Since the stiffness of the core material is low, it is very

likely that the normal forces transferred through its thickness are small, then i) can be disregarded. On the other hand, the consequences of ii) are still not very clear and they will be addressed in the following.

3.1 Composite material

It was shown in (Saravia et al., 2015b) that using a uniaxial stress constitutive formulation it is possible to obtain very accurate results. For brevity reasons, the development of the constitutive formulation will not be presented here but the reader can refer to for a detailed development of the mechanical relation of the composite material.

The constitutive relations at the layer level can be written as

$$\begin{bmatrix}\sigma_x \\ \tau_{xs}\end{bmatrix} = \begin{bmatrix}A_{11} & A_{13} \\ A_{13} & A_{33}\end{bmatrix}\begin{bmatrix}\epsilon_x \\ \gamma_{xs}\end{bmatrix}, \tag{16}$$

being A_{ij} certain elastic constants.

Recalling Eq. (15) the constitutive equations can be expressed in matrix form as

$$\boldsymbol{\sigma}_s = \boldsymbol{C}\,\boldsymbol{D}_s\boldsymbol{\varepsilon} \tag{17}$$

where

$$\boldsymbol{\sigma} = \begin{bmatrix}\sigma_x \\ \tau_{xs}\end{bmatrix}, \qquad \boldsymbol{C} = \begin{bmatrix}A_{11} & A_{13} \\ A_{13} & A_{33}\end{bmatrix}, \qquad \boldsymbol{D}_s = \begin{bmatrix}\boldsymbol{1} & \boldsymbol{r} \\ \hat{\boldsymbol{s}} & r_n\boldsymbol{1}\end{bmatrix} \tag{18}$$

The expression (17) is the constitutive equation that will be used for the calculation of the cross sectional properties of the composite blade. It must be noted that this expression could be considered equivalent to the uniaxial stress equation.

The cross sectional properties of the blade are derived with the help of the virtual work of the elastic forces; its 3D version is given by

$$\delta W_i = \int_V \delta\boldsymbol{e}^T\boldsymbol{\sigma}\, dV. \tag{19}$$

Recalling Eqs. (17) the internal virtual work of the composite blade is written as

$$\begin{aligned}\delta W_i &= \int_V \delta(\boldsymbol{D}_s\,\boldsymbol{\varepsilon})^T\boldsymbol{C}\,\boldsymbol{D}_s\,\boldsymbol{\varepsilon}\, dV \\ &= \int_V \delta\boldsymbol{\varepsilon}^T\boldsymbol{D}_s^T\boldsymbol{C}\,\boldsymbol{D}_s\,\boldsymbol{\varepsilon}\, dV\end{aligned} \tag{20}$$

The generalized strain vector is only a function of the running length coordinate of the blade, i.e. x, so the above equation can be recast in the following form

$$\delta W_i = \int_L \delta\boldsymbol{\varepsilon}^T\left(\int_A \boldsymbol{D}_s^T\boldsymbol{C}\,\boldsymbol{D}_s\, dA\right)\boldsymbol{\varepsilon}\, dx, \tag{21}$$

being the term in parentheses is the cross sectional stiffness of the blade

$$\mathbb{D} = \int_A \boldsymbol{D}_s^T\boldsymbol{C}\,\boldsymbol{D}_s\, dA. \tag{22}$$

Its explicit form is

$$\mathbb{D} = \int_A \begin{bmatrix} \mathbf{1}^T & \hat{\boldsymbol{s}}^T \\ \boldsymbol{r}^T & r_n^\omega \mathbf{1}^T \end{bmatrix} \begin{bmatrix} A_{11} & A_{13} \\ A_{13} & A_{33} \end{bmatrix} \begin{bmatrix} \mathbf{1} & \boldsymbol{r} \\ \hat{\boldsymbol{s}} & r_n^\omega \mathbf{1} \end{bmatrix} dA. \tag{23}$$

where $r_n^\omega = r_n + \omega_s'$.

3.2 Discretization and segment reconstruction

The outer contour of a wind turbine blade is fixed by aerodynamic requirements; it is given as a set of points in the two dimensional space. The aerodynamic table can be easily converted to lines and then imported into a meshing software to generate the set of two dimensional line segments. A LLA takes the line-discretized aerodynamic profile of the blade and the shear web locations from an input file. The file also contains the material mapping table; this implies the definition of the material constants, lamination sequence and thickness distribution.

After the discretization process, each segment must be projected inwards in the direction of the surface normal in order to reconstruct the actual blade geometry. To perform this operation several possibilities can be devised; in this paper, reconstruction with rectangles and trapezoids will be studied. Surprisingly, the impact of the geometric description of the cross section in the accuracy of the thin-walled theory has not been addressed before; this will be shown to be of key importance for obtaining accurate results.

As already said, the outer contour of the cross section is given a priori by the aerodynamic design of the blade. From the geometric point of view, it is relevant the fact that the inner layers of a segment of laminate have not the same length than the outer layers. This may result trivial, but this point is rarely considered in thin-walled beam theory. Of course, the effect of the curvature variation disappears as the thickness of the laminate tends to zero; but as stated, at some locations of the cross section the wall is very thick due to the necessity of increasing the local buckling strength.

The reconstruction of the blade geometry must done via projection of the inward normal of the outer contour according to the information given in the lamination table. This opens the possibility for a reconstruction with three segment types: i) unmatching rectangles, ii) matching trapezoids and iii) unmatching trapezoids; see Figure 1. Unmatching rectangles are constructed through normal projection in the direction of the segment normal; matching trapezoids are constructed using the intersection point of the inner layers, thus avoiding thickness discontinuity; finally, unmatching trapezoids are obtained through projection in the direction of the average nodal normal.

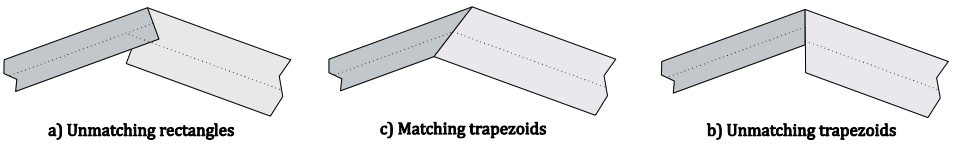

Figure 1 – LLA Segments

At first sight there are two observations that could be made from Figure 1. Firstly, option i) should overestimate the cross section properties; this is a fact since the reconstruction clearly duplicate the intersection area. Secondly, option ii) should give the most accurate representation of an actual thickness transition; but this depends on the actual nature of the joint between the segments, which cannot be universally defined. There exist some drawbacks that makes the matching trapezoid not suitable for the geometric reconstruction of unmatching thickness joints; the next paragraphs clarify this.

Firstly, the geometrical aspects of a joint constructed with matching trapezoids are analyzed. Although it may seem trivial to construct a matching trapezoidal joint from the one dimensional mesh of segments, it takes some effort to derive the location of the intersection point of the inner contours of two contiguous segments. Figure 2 shows the typical case where element number 1 and element number 2 inner mid-contours meet at an undetermined point *p*.

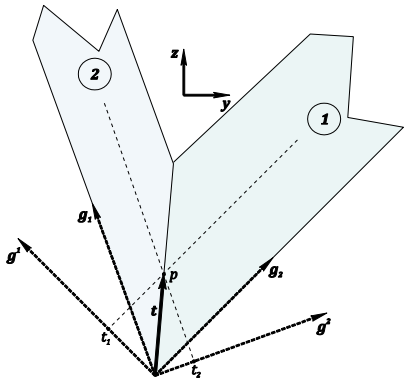

Figure 2 – Matching trapezoid joint

Here the unknown is the mid-point vector $\boldsymbol{t}$, which permits to locate the mid-contours intersection point. Surprisingly, it seems like there is no easy vectorial shortcut to $\boldsymbol{t}$; and posing the problem in non-orthogonal coordinates cannot be avoided. The relative location of the intersection of the mid-contours can be found as

$$\boldsymbol{t} = t_1\boldsymbol{g}^1 + t_2\boldsymbol{g}^2, \tag{24}$$

where $\boldsymbol{g}^i$ is a non-orthogonal basis with unit vectors that are defined from the segment perpendicular vectors. Then, t_i are the covariant components of $\boldsymbol{t}$ in the base $\boldsymbol{g}^i$. The definition of a reciprocal basis such that $\boldsymbol{g}_i \cdot \boldsymbol{g}^j = \delta_i^j$ allows to write the covariant components as (Crisfield)

$$t_i = \bar{\boldsymbol{t}} \cdot \boldsymbol{g}_i. \tag{25}$$

where $\bar{\boldsymbol{t}}$ is the Cartesian expression of $\boldsymbol{t}$, i.e. $\bar{\boldsymbol{t}} = \left(c_1\check{\boldsymbol{\jmath}} + c_2\check{\boldsymbol{k}}\right)$. Then it is possible to obtain

$$t_i = \left(c_1\check{\boldsymbol{\jmath}} + c_2\check{\boldsymbol{k}}\right) \cdot \boldsymbol{g}_i, \tag{26}$$

which gives the following algebraic equation

$$\begin{bmatrix} t_1 \\ t_2 \end{bmatrix} = \begin{bmatrix} \check{\boldsymbol{\jmath}} \cdot \boldsymbol{g}_1 & \check{\boldsymbol{k}} \cdot \boldsymbol{g}_1 \\ \check{\boldsymbol{\jmath}} \cdot \boldsymbol{g}_2 & \check{\boldsymbol{k}} \cdot \boldsymbol{g}_2 \end{bmatrix} \begin{bmatrix} c_1 \\ c_2 \end{bmatrix}. \tag{27}$$

This can be written as

$$t_i = \mathcal{M}^{ij} c_j, \tag{28}$$

and finally find the Cartesian components of $\boldsymbol{t}$ as

$$c_i = \mathcal{M}^{ji} t_j. \tag{29}$$

Once the coefficients are determined, both the inner and mid-contour intersections are easily calculated.

But $\boldsymbol{\mathcal{M}}^{ij}$ is singular when $\boldsymbol{g}_1$ and $\boldsymbol{g}_2$ are linear combination of each other. Geometrically, this is equivalent to both segments being collinear (or almost collinear); a very common situation for most aerodynamic discrete profiles. This would imply that there is no answer to c_i, and thus the algorithmic version of the above formulation crashes.

If the two segments have the same thickness, the situation can be saved; the calculation of the vector can be bypassed through the simple formula

$$\bar{\boldsymbol{t}} = -\frac{1}{2}\, e \cdot \breve{\boldsymbol{n}}, \tag{30}$$

where e is the thickness of the laminate and $\breve{\boldsymbol{n}}$ is the outward normal. But if the thicknesses of the elements are not equal, then there is no way to find c_i without exploiting Eq. (29). This situation is depicted in Figure 3, where clearly at locations A and B the matching trapezoid squeme would fail to give a joint intersection point.

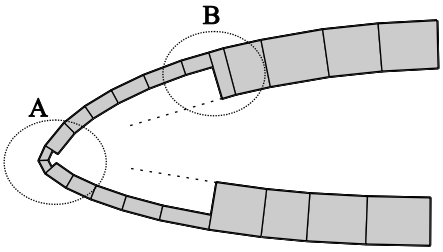

Figure 3 – Joint Geometry

So, although a joint without a thickness discontinuity may seem attractive at first sight, it is not always a good alternative to represent the laminate transitions in typical wind turbine cross sections. This is not only because the intersection point between the neighbor segments cannot exist, but also, because although it is guaranteed that it exists, the represented joint may not be similar to real.

In virtue of the above comments, it is concluded that the matching trapezoid is not a good choice to reconstruct blade cross sections with large thickness changes.

4 NUMERICAL TESTS

This section presents the performance of the formulation in several practical tests, which were carefully designed to compare the modeling capabilities of existing cross sectional stiffness calculation codes (Chen et al., 2010). The presented formulation was implemented computationally in a Python code called CXS.

All comparisons are made assuming that VABS (Cesnik and Hodges, 1997) results are the baseline; this is justified by the fact that both its formulation and implementation are based on a SLA. For the sake of brevity, only relevant geometric and material data of each example are presented here, the reader can refer to (Chen et al., 2010) for further details. In some examples, results obtained the LLA PreComp are presented; PreComp was chosen to benchmark the present formulation mainly because it is the most used LLA (Saravia et al., 2015a, Chen et al., 2010).

4.1 Thick-walled isotropic tube

The first example is set to test the performance of the algorithm in an extreme thick-walled cross section; an isotropic circular aluminum tube with a thickness to diameter ratio of 1/3 is the chosen geometry. VABS and PreComp results are used to benchmark the present algorithm.

The results are presented in Table 1; they show an excellent agreement between VABS and CXS trapezoidal element; both the stiffness and mass coefficients agree with an error less than 1%.

	VABS	PreComp (Chen et al., 2010)	CXS Trapezoids 10 layers	CXS Trapezoids 5 layers	CXS Rectangles 10 layers
Axial	1.834×10^{10}	2.750×10^{10}	1.834×10^{10}	1.834×10^{10}	2.751×10^{10}
Bending	4.587×10^{8}	5.936×10^{8}	4.575×10^{8}	4.556×10^{8}	5.958×10^{8}
Torsion	3.449×10^{8}	4.115×10^{8}	3.439×10^{8}	3.424×10^{8}	4.476×10^{8}
Mass	7.037×10^{2}	1.055×10^{3}	7.034×10^{2}	7.034×10^{2}	1.055×10^{3}
I1	3.519×10^{1}	-	3.509×10^{1}	3.495×10^{1}	4.570×10^{1}
I2 – I3	1.759×10^{1}	2.280×10^{1}	1.755×10^{1}	1.747×10^{1}	2.285×10^{1}

Table 1– Thick-walled tube cross sectional properties.

There are some important conclusions that can be drawn from the experiment; i) the trapezoidal segment can reconstruct exactly the geometry, ii) layering do not improve significatively the predictions, iii) the rectangular element do not predict well any of the cross sectional parameters, iv) the PreComp results agree exactly with those of the CXS rectangles. The latter strongly suggests that PreComp errors are very likely due to insufficient geometric detailing.

In virtue of the above, it must be strongly remarked that for the problem at hand the source of error of the LLAs is purely geometric; when the geometry is modeled correctly, as done by CXS trapezoids, the errors dissapear. The CXS trapezoidal element geometric reconstruction of the thck-walled tube can be seen in Figure 4.

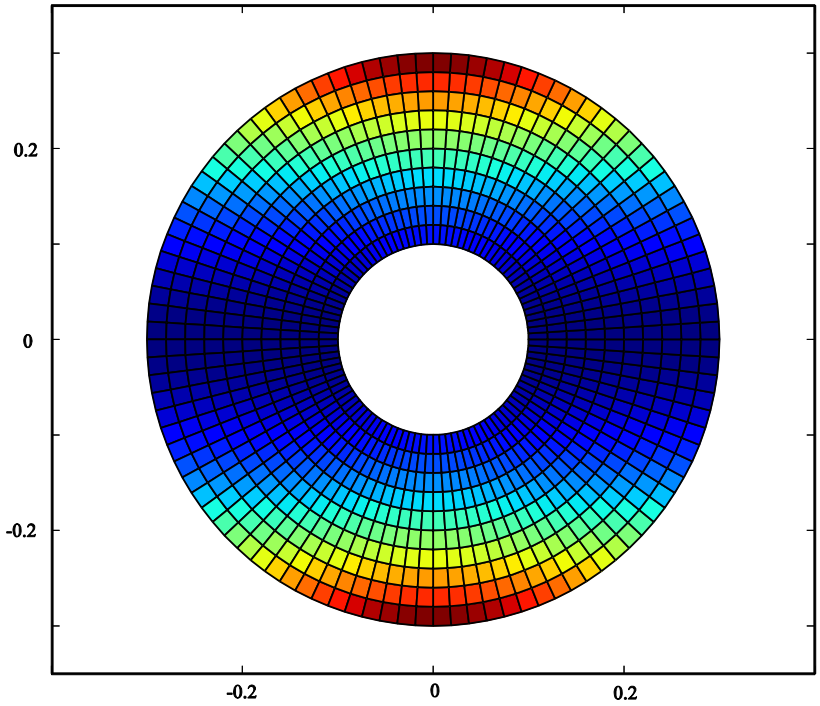

Figure 4 – Thick-walled tube (bending stiffness colormap).

4.2 Isotropic blade-like section

In the previous example, the performance of the algorithm in a thick-walled cross section was tested; since the material was isotropic and the cross section was bisymmetric, there were no stiffness or mass coupling terms in the stiffness matrix. In order to test the influence of the geometrical terms in the stiffness coupling a monosymmetric isotropic section is used; then the analytical blade-like section proposed by Chen et al. (Chen et al., 2010) is tested.

	VABS	PreComp (Chen et al., 2010)	CXS Trapezoids	CXS Rectangles	CXS Error
Axial	3.551×10^{7}	3.794×10^{7}	3.551×10^{7}	3.778×10^{7}	0.0%
Flap Bending	2.088×10^{9}	2.178×10^{9}	2.088×10^{9}	2.161×10^{9}	0.0%
Lag Bending	1.108×10^{10}	9.100×10^{9}	1.108×10^{10}	1.292×10^{10}	0.0%
Torsion	2.006×10^{9}	1.696×10^{9}	1.951×10^{9}	2.070×10^{9}	2.7%
Ext-Bend	-3.381×10^{8}	-3.238×10^{8}	-3.381×10^{8}	-3.821×10^{8}	0.0%
Mass	1.841×10^{-7}	1.960×10^{-7}	1.843×10^{-7}	1.960×10^{-7}	0.1%
I1	6.826×10^{-5}	-	6.831×10^{-5}	7.828×10^{-5}	0.1%
I2	1.082×10^{-5}	1.125×10^{-5}	1.083×10^{-5}	1.121×10^{-5}	0.1%
I3	5.743×10^{-5}	4.702×10^{-5}	5.747×10^{-5}	6.707×10^{-5}	0.0%
Tension Center	9.521	10.000	9.521	10.114	0.0%

Table 2 –Isotropic blade-like section cross sectional properties.

Inspecting Table 2 the same behavior as the previous example is observed. The following comments can be made: i) the accuracy of CXS trapezoids is excellent, ii) the CXS rectangles overestimate the parameters due to duplication of the segment intersection, iii) the CXS rectangles and PreComp give very similar results, iv) the lag stiffness and inertia results for

PreComp do not show the classical overestimation; it is suspected that a modeling error is present in the results presented in (Chen et al., 2010), v) PreComp is not very consistent, some variables are over-predicted and others are under-predicted, vi) again, the CXS trapezoids are more flexible than VABS only in torsion. The latter is expected since the present formulation neglects hoop moments (Hodges, 2006). The CXS trapezoidal element geometric reconstruction of the blade-like section can be seen in Figure 5.

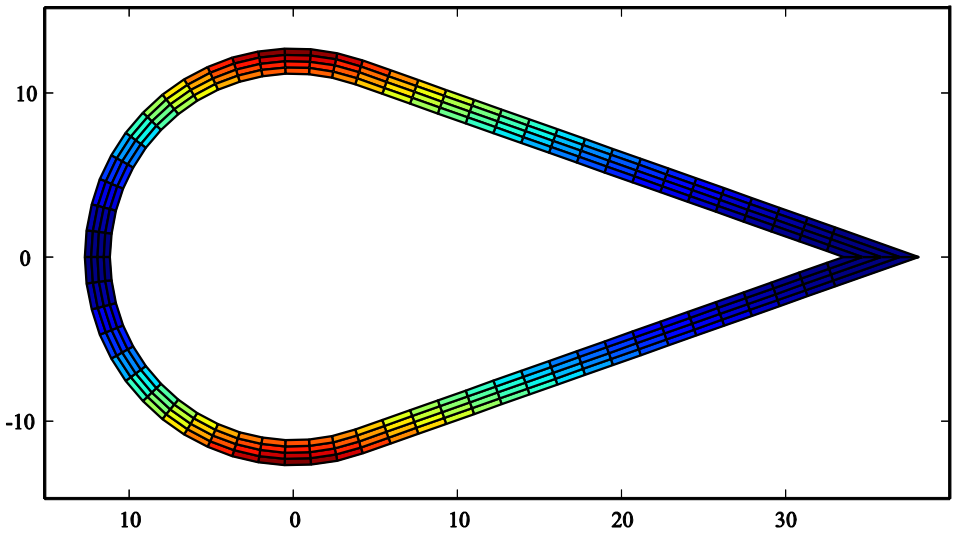

Figure 5 – Blade-like section (bending stiffness colormap).

4.3 Anisotropic oval pipe

This example consist on a multi-layer composite pipe with oval shape (Saravia et al., 2015a), see Figure 4. The pipe is thick-walled and anisotropic; the lamination stacking sequence is unsymmetrical and unbalanced.

Besides VABS results, PreComp data presented in (Chen et al., 2010) will be used to benchmark the present formulation. It must be noted that in (Chen et al., 2010), dimensioning of the inner and middle radiuses of the oval is incorrect; the total thickness of the cross section is 5.08 mm instead of 2.54 mm. Also the material properties were wrongly informed, the constants used in the calculations are: E_{11}=141.963 GPa, E_{22}= E_{33}=9.79056 GPa, G_{12}= G_{12}= G_{23}=5.9984 GPa.

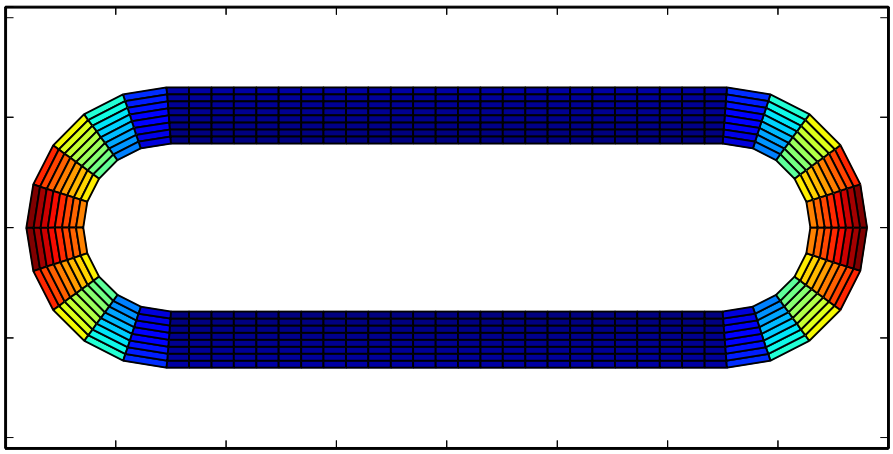

Figure 6 – Anisotropic oval pipe (bending stiffness colormap).

This is a very unfavorable section for the present formulation because the lamination sequence is not balanced and circumferentially asymmetric, then the errors that arise from the neglecting of the circumferential curvature are maximized.

	VABS	PreComp	CXS Trap.	CXS Rect.	Error CXS Trap.	Error CXS Rect.
Axial	4.606×10^{7}	7.833×10^{7}	4.580×10^{7}	4.760×10^{7}	0.5%	3.3%
Bending 1	5.378×10^{3}	7.074×10^{7}	5.355×10^{3}	5.444×10^{3}	0.4%	1.2%
Bending 2	1.532×10^{4}	4.857×10^{4}	1.530×10^{4}	1.704×10^{4}	0.1%	11%
Torsion	1.959×10^{3}	8.628×10^{3}	1.722×10^{3}	2.132×10^{3}	12%	8.8%
Ext-Bend 2	2.088	-	1.856	-3.028×10^{-1}	11%	12%
Ext-Bend 1	-4.117	-	-3.856	-1.314	6%	6%
Ext-Tors	1.079×10^{4}	-1.205×10^{-2}	1.258×10^{4}	4.420×10^{3}	16%	16.5%
Mass	8.957×10^{1}	-	8.957×10^{1}	8.830×10^{1}	0.0%	0.0%
I1	5.499×10^{-4}	-	5.498×10^{-4}	5.599×10^{-4}	0.0%	0.0%
I2	7.661×10^{-5}	-	7.660×10^{-5}	8.046×10^{-5}	0.0%	0.0%
I3	4.733×10^{-4}	-	4.732×10^{-4}		0.0%	

Table 3 – Anisotropic oval pipe cross sectional properties.

Despite the above comments, the Table 3 shows that the trapezoidal element still has a very good performance; for the most critical terms, the extensional-bending and the extensional-torsional couplings, the results are acceptable.

The maximum error is that of the extensional-torsional coupling; this error is 16%, far below the error reported in (Chen et al., 2010) for other one dimensional codes; best is Pre-Comp, predicting an extensional torsional coupling of -1.2×10^{-2}. This represents an error of six orders of magnitude. Again, the CXS rectangle element is not as accurate as the trapezoid; although the results are consistent; both CXS elements give better results than PreComp.

From the observation of the torsional values, an important remark can be made. Compared to VABS, the trapezoidal element predicts a lower torsional stiffness (12% error) while the rectangular element predicts a higher stiffness (8.8% error). Although at first glance it could be said that the rectangular element has a better performance, this is not so. The prediction of the torsional stiffness of a CAS laminated cross section done by an algorithm without significant geometrical errors should be below the real value; this is because the zero hoop moment assumption flexibilizes the cross section (Hodges, 2006). This flexibilization is also present in the rectangular element, but since the rectangular element overestimates areas, this overcompensates the flexibilization caused by the zero hoop moment assumption. Thus, it is very important to note that although the torsional stiffness error is lower in the rectangular element, the prediction is clearly worse.

4.4 The MH104 wind turbine blade (Chen et al., 2010)

In this example a real wind turbine cross section is analyzed; the cross section is presented in (Chen et al., 2010). Geometrical and material data details can be found in the mentioned reference. In order to facilitate the VABS modeling, both the Gelcoat and the Nexus layers were removed from the model. This affects slightly the mass and inertia constants, but otherwise the VABS model would be very difficult to generate. The Figure 7 shows the geometry of the MH104 blade.

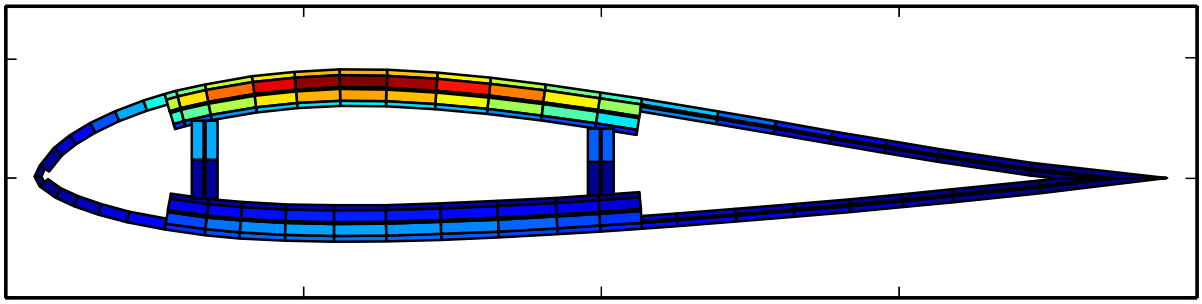

Figure 7 – MH104 blade (bending stiffness colormap).

The stiffness and mass results are presented in Table 4. It can be seen that the trapezoidal elements give a better prediction than the rectangles. The following comments can be made: i) the axial, flap and lag stiffness is overpredicted by both elements, ii) the torsional stiffness is underpredicted by both elements; this is due to disregarding hoop moments iii) the torsional stiffness error of the rectangular element is smaller than that the trapezoidal element; this is caused by the stiffening caused by the duplication of areas of the rectangle element, iv) all coupling terms are very well predicted, v) the mass and inertia terms are prediction with trapezoidal elements gives the same results as VABS.

	VABS	CXS Trapezoids	CXS Rectangles	Error Trapezoids	Error Rectangles
Axial	2.443×10^{9}	2.547×10^{9}	2.616×10^{9}	4.2%	7.1%
Flap	2.164×10^{7}	2.301×10^{7}	2.330×10^{7}	6.3%	7.6%
Lag	4.683×10^{8}	4.887×10^{8}	5.338×10^{8}	4.3%	13.9%
Torsion	2.693×10^{7}	2.24×10^{7}	2.344×10^{7}	-16.8%	-12.9%
Ext-Flap	7.006×10^{7}	7.263×10^{7}	7.411×10^{7}	3.6%	5.7%
Ext-Lag	-4.695×10^{8}	-4.900×10^{8}	-4.631×10^{8}	4.3%	-1.3%
Ext-Tors	-3.293×10^{7}	-2.986×10^{7}	-2.937×10^{7}	-9.3%	-10.8%
Mass	2.601×10^{2}	2.603×10^{2}	2.693×10^{2}	0.0%	3.5%
I1	5.620×10^{1}	5.619×10^{1}	6.255×10^{1}	-0.0%	11.2%
I2	5.381×10^{1}	5.380×10^{1}	6.013×10^{1}	-0.0%	11.7%
I3	2.381	2.385	2.415	0.1%	1.4%

Table 4 – MH104 blade cross sectional properties.

Observing the results presented in (Chen et al., 2010) and (Saravia et al., 2015a) and comparing with the present results it can be seen that the results are very sensitive to modeling details. In order to alleviate this issue the above calculations were generated with exactly the same geometrical data.

4.5 Sandia SNL100-3 Blade

Sandia National Laboratories have been working intensively in the design of a 100 meter wind turbine blade concept (Griffith and Ashwill, 2011, Griffith and Richards, 2014); up to date, this is the largest blade in the world. The last design, named SNL100-3, incorporates carbon fiber and flat-back airfoils. In this example the results of the blade stiffness and mass parameters at the maximum chord station of the Sandia SNL100-3 blade are presented. The blade geometry is shown in Figure 8.

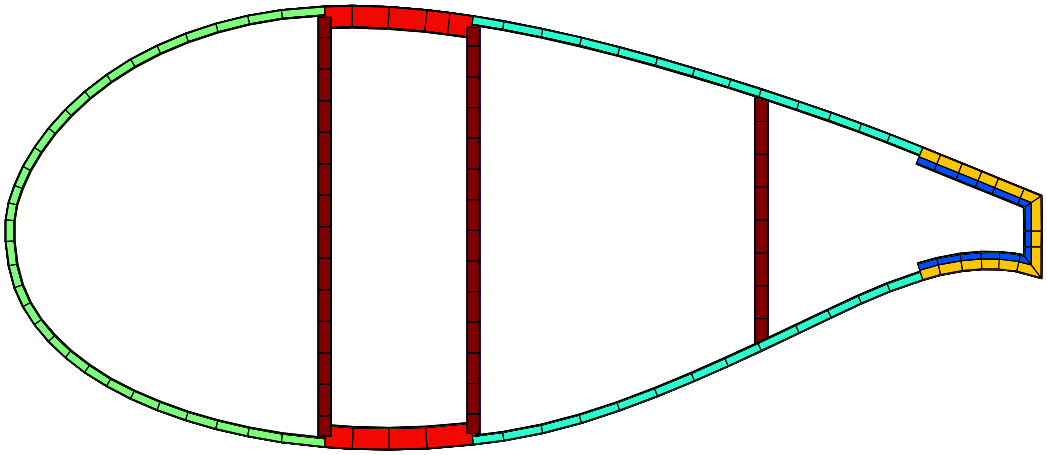

Figure 8 – SNL100-8 blade (station 18).

As usual, the benchmark is done taking VABS as baseline. Both the VABS and the CXS models were generated using the geometric and material data published by Sandia, while the Pre-Comp results are taken from the Sandia report (Griffith and Richards, 2014).

	VABS	Pre-Comp (Griffith and Richards, 2014)	CXS Rectangles	CXS Trapezoids	Error (%)		
					PreComp	CXS Rect.	CXS Trap.
Axial	2.349×10^{10}	2.425×10^{10}	2.427×10^{10}	2.375×10^{10}	3.2	3.3	1.1
Flap	2.109×10^{10}	2.193×10^{10}	2.160×10^{10}	2.128×10^{10}	4.0	2.4	0.9
Lag	3.685×10^{10}	3.390×10^{10}	3.951×10^{10}	3.700×10^{10}	-8.0	7.2	0.4
Torsion	1.526×10^{10}	1.342×10^{9}	1.551×10^{9}	1.507×10^{9}	-12.1	1.6	-1.2
Mass	6.534×10^{2}	6.803×10^{2}	6.793×10^{2}	6.627×10^{2}	4.1	4.0	1.4
Flap Inertia	3.708×10^{2}	3.908×10^{2}	3.823×10^{2}	3.789×10^{2}	5.4	3.1	2.2
Lag Inertia	2.118×10^{3}	1.617×10^{3}	2.269×10^{3}	2.127×10^{3}	-23.7	7.1	0.4
x_{tc}	0.473	0.485	0.488	0.468	2.5	3.2	-1.1

Table 5 –Sandia SNL100-3 blade cross sectional properties.

From the results are presented in Table 5 the following comments can be made: i) CXS trapezoids give better results than CXS rectangles and PreComp, ii) CXS is consistent in the sense that it overpredicts the stiffness and mass parameters; except for the torsional stiffness, which is, as usual, underpredicted; this is because the formulation neglects the hoop moments, iii) PreComp is not consistent, some parameters are overpredicted while others are underpredicted.

As a closing remark, it is mentioned that VABS computing time was 309 seconds while CXS computing time was 0.1 second. Besides, generation of the VABS model took approximately 6 hours, while the CXS model took 20 minutes.

5 CONCLUSIONS

Computing the cross sectional stiffness and inertia properties of realistic composite blades via a line-line algorithm (LLA) has been proven to be very effective. Different benchmark tests were performed and a detailed comparison of the most important inertia and stiffness terms was done. It was shown that the simplest version of the classical lamination theory can yield accurate results if the cross section is well represented geometrically.

The blade reconstruction via two segments has been studied, unmatching rectangles and unmatching trapezoids. The unmatching trapezoid segment has shown an excellent

performance, being very accurate and algorithmically stable. This element can reconstruct effectively extremely thick-walled sections as well as sections with discontinuous thickness distributions. It was shown that the stiffness and mass matrices have shown an excellent agreement with VABS. Also the coupling stiffness terms and the tension centers have been predicted with small errors. The torsional stiffness terms are the most prone to errors, the maximum error found for the torsional stiffness is around 12%.

ACKNOWLEDGEMENTS

The authors with to acknowledge the supports from Grupo de Investigación en Multifísica Aplicada at Universidad Tecnológica Nacional, CONICET and FONCYT. This work was supported by Prestamo BID PICT 2013 1146 FONCYT.

REFERENCES

Bir, G., User's Guide to PreComp. http://wind.nrel.gov/designcodes/preprocessors/precomp/PreComp.pdf: National Renewable Energy Laboratory, 2005.

Cesnik, C. E. S. & Hodges, D. H. VABS: A New Concept for Composite Rotor Blade Cross-Sectional Modeling. *Journal of the American Helicopter Society,* 42**,** 27-38, 1997.

Chen, H., Yu, W. & Capellaro, M. A critical assessment of computer tools for calculating composite wind turbine blade properties. *Wind Energy,* 13**,** 497-516, 2010.

Crisfield, M. A. *Non-Linear Finite Element Analysis of Solids and Structures: Advanced Topics*, John Wiley & Sons, Inc., 1997.

Griffith, D. T. & Ashwill, T. D., The Sandia 100-meter all-glass baseline wind turbine blade: SNL100-00. Sandia National Laboratories, 2011.

Griffith, D. T. & Richards, P. W., The SNL100-03 Blade: Design Studies with Flatback Airfoils for the Sandia 100-meter Blade. Sandia National Laboratories, 2014.

Hansen, M. O. L. *Aerodynamics of Wind Turbines,* London, Earthscan Publications Ltd., 2008.

Hansen, M. O. L., Sørensen, J. N., Voutsinas, S., Sørensen, N. & Madsen, H. A. State of the art in wind turbine aerodynamics and aeroelasticity. *Progress in Aerospace Sciences,* 42**,** 285-330, 2006.

Hau, E. *Wind Turbines,* Berlin, Springer, 2006.

Hodges, D. H. *Nonlinear Composite Beam Theory,* Virginia, American Institute of Aeronautics and Astronautics, Inc., 2006.

Hodges, D. H. & Yu, W. A rigorous, engineer-friendly approach for modelling realistic, composite rotor blades. *Wind Energy,* 10**,** 179-193, 2007.

Jonkman, J. M., Butterfield, S., Musial, W. & Scott, G., Definition of a 5-MW Reference Wind Turbine for Offshore System Development. National Renewable Energy Laboratory, 2009.

Laird, D. L., NuMAD User's Manual. Sandia National Laboratories, 2001.

Lindenburg, C., STABLAD. Stability analysis tool for anisotropic rotor blade panels. Energy Research Center of the Netherlands, 2008.

Malcolm, D. J. & Laird, D. L. Extraction of equivalent beam properties from blade models. *Wind Energy,* 10**,** 135-157, 2007.

Philippidis, T. P., Vassilopoulos, A. P., Katopis, K. P. & Voutsinas, S. G. A software for fatigue design and analysis of composite rotor blades. . *Wind Engineering,* 20**,** 349-362, 1996.

Resor, B. & Paquette, J. Published. Uncertainties in prediction of wind turbine blade flutter. Structural Dynamics and Materials Conference, 2011 Denver, Colorado. American Institute of Aeronautics and Astronautics, 2011.

Resor, B., Paquette, J., Laird, D. L. & Griffith, D. T. Published. An evaluation of wind turbine blade cross section analysis techniques. 18th Structural Dynamics and Materials Conference, 2010 Orlando, Florida. American Institute of Aeronautics and Astronautics, 2010.

Saravia, M. C. A large deformation-small strain formulation for the mechanics of geometrically exact thin walled beams *Thin-Walled Structures,* In Press, 2014.

Saravia, M. C., Saravia, L. J. & Cortínez, V. H. A one dimensional discrete approach for the determination of the cross sectional properties of composite rotor blades. *Renewable Energy,* 80**,** 713-723, 2015a.

Saravia, M. C., Saravia, L. J. & Cortínez, V. H. A one dimensional discrete approach for the determination of the cross sectional properties of composite rotor blades. *Renewable Energy,* 80**,** 713-723, 2015b.

Spera, D. A. (ed.) 2009. *Wind Turbine Technology,* New York: ASME.

UpWind, Design limits and solutions for very large wind turbines. http://www.upwind.eu/, 2011.

Yu, W., Volovoi, V. V., Hodges, D. H. & Hong, X. Validation of the variational asymthotic beam sectional analysis. *IAA Journal,* 40**,** 2105-2113, 2002.